

**GT2004-53971****INTRODUCTION OF RESIDUAL STRESSES TO ENHANCE FATIGUE  
PERFORMANCE IN THE INITIAL DESIGN**

Paul Prev y (pprevey@lambda-research.com)  
Lambda Research, Cincinnati, OH 45227

N. Jayaraman (njayaraman@lambda-research.com)  
Lambda Research, Cincinnati, OH 45227

Ravi Ravindranath (ravi.ravindranath@navy.mil)  
NAVAIR, Patuxent River, MD 20670

**ABSTRACT**

High cycle fatigue (HCF) performance of turbine engine components has been known for decades to benefit from compressive surface residual stresses introduced through shot peening. However, credit for the fatigue benefits of shot peening has not been taken into account in the design of components. Rather shot peening has been used primarily to safe guard against HCF damage initiation. Recently, laser shock processing (LSP) and low plasticity burnishing (LPB) have been shown to provide spectacular fatigue and damage tolerance improvement by introducing deep (through-thickness) compression in critical areas. Until now, the fatigue benefits of these new surface treatments have been introduced during repair to improve an existing design. The present paper describes a design methodology and testing protocol\* to take appropriate credit for the introduction of beneficial residual stresses into a component design to achieve optimal fatigue performance.

A detailed design protocol has been developed that relates the introduction of a residual stress distribution using LPB for targeted HCF performance. This design protocol is applied to feature specimens designed to simulate the fatigue conditions at the trailing edge of a 1<sup>st</sup> stage low pressure compressor vane to provide optimal trailing edge damage tolerance. The use of finite element modeling, linear elastic fracture mechanics, and x-ray diffraction documentation of the residual stress field to develop LPB processing parameters is described. A novel adaptation of the traditional Haigh diagram to estimate the compressive residual stress magnitude and distribution to

achieve optimal fatigue performance is described. Fatigue results on vane-edge feature samples are compared with analytical predictions provided by the design methodology. The potential for designing reduced section thickness of structural components leading to weight savings is discussed.

**INTRODUCTION**

The benefits of residual compressive stresses to enhance fatigue strength in metallic components have long been recognized.<sup>1-4</sup> Many engineering components have been shot-peened or cold worked with fatigue strength enhancement as the primary objective. Beneficial surface compression may also be achieved as a by-product of a surface hardening treatment like carburizing/nitriding. Over the last decade, new surface treatments like LPB,<sup>5</sup> LSP,<sup>6</sup> and ultrasonic peening have emerged. All of these surface treatment methods have been shown to benefit fatigue prone components to different degrees.

LPB has been demonstrated to provide a deep, thermally and mechanically stable, surface layer of high magnitude compression in aluminum, titanium, nickel based alloys and steels. Thermal and mechanical stability are obtained when deep compression is achieved with minimal cold work of the surface. The deep stable compressive residual stress state on the surface of these materials has been shown to be effective in mitigating fatigue damage due to foreign object damage (FOD),<sup>7-9</sup> fretting,<sup>10-11</sup> and pitting/corrosion.<sup>12-15</sup>

Since shot peening yields only a shallow layer of surface compression (< 0.25 mm deep), and can relax rapidly in

service, no design credit for the beneficial compression is generally taken. The fatigue community has generally used shot peening only for an additional safety margin and not as a design methodology. In contrast, the new surface treatment processes have enabled imparting deeper stable compressive residual stress layers, thus mitigating the adverse effects of defects, cracks and pits. Through processes like LPB and LSP, compressive residual stresses are imparted on component surfaces to a depth greater than 1 mm. This enables complete mitigation of FOD, domestic object damage (DOD), and other surface damage including fretting, and corrosion pitting. In most cases, the fatigue performance of the virgin material is completely restored even in the presence of such defects. In the absence of compressive residual stresses, the allowable damage is generally limited to a notch severity factor ( $k_f$ ) of 3. In most engineering structural materials this design constraint leads to low allowable design stresses, and consequently use of much thicker sections.

A comprehensive approach to designing structures by taking specific design credit for surface compressive residual stresses is yet to be developed. Complete mitigation of FOD, pitting, fretting and erosion damage is possible with well-designed residual stress distributions. Additional factors including compensatory tension in the structure, part distortion and dimensional tolerance, must be taken into account in the design process. This paper proposes such a residual stress design approach with a specific case study of HCF behavior of feature specimens designed to simulate the stress conditions existing in an aircraft engine first stage compressor vane.

**STRESS-LIFE ANALYSIS**

The constant life diagram for illustrating the effects of mean stresses on HCF fatigue life, commonly known as the Haigh diagram<sup>16</sup> is schematically shown in Figure 1. This is a map of the maximum and minimum stresses for constant cyclic lives, such as  $10^4$ ,  $10^5$ ,  $10^6$ ,  $10^7$  cycles, plotted as solid curves for a given material in fatigue. The fatigue stresses ( $\sigma_{max}$  and  $\sigma_{min}$ ) are usually normalized with respect to the tensile strength of the material. It is customary to show the normalized mean stress and alternating stress axes in the same diagram, and the fatigue test results presented in this diagram are bound by these two axes. The Haigh diagram, a convenient graphical representation to show the effects of mean stress, is drawn based upon fatigue test results. Effects of fatigue notch severity factor ( $k_f = \text{unnotched } \sigma_e / \text{notched } \sigma_e$ ) are plotted as dotted lines based upon experimental results. Although Haigh's fatigue tests included compressive mean stresses, the Haigh diagrams shown subsequently in the fatigue literature did not generally include this range.

Most predictive methods like the Goodman, Gerber and Soderberg diagrams are derivatives of the Haigh diagram shown schematically in Figure 2, and are plots of stress amplitudes

plotted against mean stress. The equations that describes these lines are:

$$\sigma_a = \sigma_e \{ 1 - \sigma_m / \sigma_{YS} \} \quad \text{Soderberg equation} \quad [1]$$

$$\sigma_a = \sigma_e \{ 1 - \sigma_m / \sigma_{UTS} \} \quad \text{Goodman equation} \quad [2]$$

$$\sigma_a = \sigma_e \{ 1 - (\sigma_m / \sigma_{UTS})^2 \} \quad \text{Gerber equation} \quad [3]$$

where  $\sigma_a$  is the allowable alternating stress,  $\sigma_e$  is the fully reversed fatigue strength at R ( $\sigma_{min}/\sigma_{max}$ ) = -1, and  $\sigma_m$  is the mean stress at which the allowable alternating stress is determined. Thus, these predictive models are essentially lines between experimentally determined fatigue strength in fully reversed cyclic loading condition (R = -1) for a predetermined cyclic life (say,  $10^7$  cycles), and yield or tensile strength of the material.

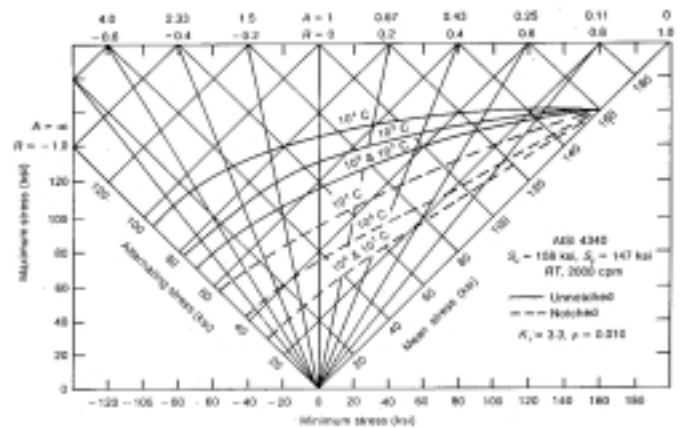


Figure 1 – Master diagram for establishing influence of mean stress in fatigue (from MIL-HBDK-5, US Dept. of Defense) (Dieter (1986), Mechanical Metallurgy, McGraw-Hill, Third Edition pg. 386, Figure 12-9.)

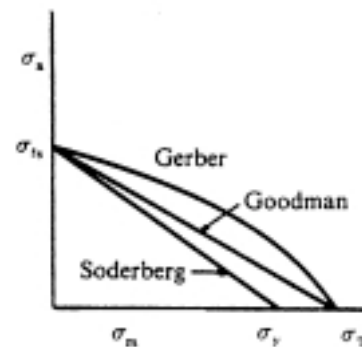


Figure 2 – Constant life curves for fatigue loading with nonzero mean stress. (Suresh (1998), Fatigue of Materials, Cambridge University Press, Second Edition, pg. 226, Figure 7.4 (b))

Experimental investigations of the effect of compressive mean stresses were attempted in the 1950s and 1960s with

varying success. Most of these researchers acknowledged the difficulties with specimen alignment in their fatigue tests and therefore, the use of this data for purposes of extending the Haigh diagram or the Goodman line into the compressive mean stress region was not seriously considered. However, in one of the early attempts, O'Connor and Morrison<sup>17</sup> showed the construction of a diagram with a triangular bounding region to indicate the limits of applied stresses, in both the tensile and compressive mean stress regions. Fatigue test results were summarized in a triangle (shown in Figure 3) with the three corners represented by the mean stress ranging from compressive yield to tensile yield strength, and the alternating stress ranging from zero to the yield strength of the material (for Ni-Cr-Mo alloy carbon steel). The implications are that the boundaries set by the triangle are indeed the limit to which stresses may be applied, without yielding, under any circumstance. Fatigue strength data plotted in this space further bounds the upper limits of allowable mean and cyclic stresses.

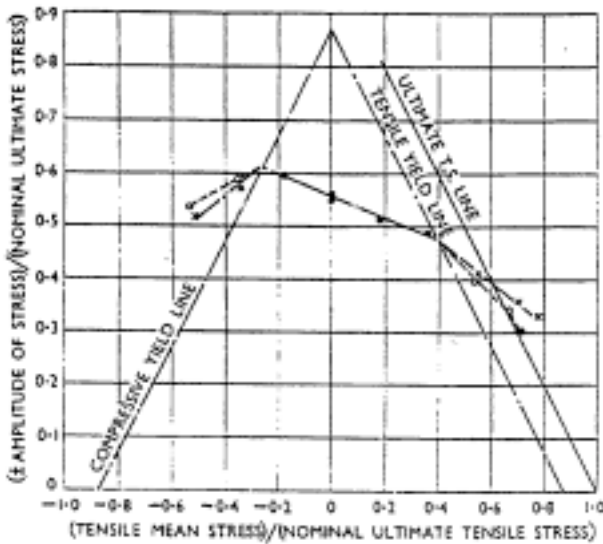


Fig. 2.26. Summary of Results

○ Nominal      × Actual      ● No measurable yielding  
 ■ Results from tests in reversed bending (Morrison, Crossland, and Parry)

Figure 3 – Summary of results. (H.C. O'Connor, J.L.M. Morrison, (1956), "The Effect of Mean Stress on the Push-Pull Fatigue Properties of an Alloy Steel," Intn'l Conf. on Fatigue, Inst. Of Mechanical Engineers, pg. 108, Figure 2.26.)

Due to limitations mentioned earlier in experimental verification of fatigue behavior under high compressive mean stresses, neither the Haigh, nor the Goodman representations of fatigue diagrams have been reliably used to predict the fatigue performance under loading conditions of  $R < -1$ , i.e., with compressive mean stresses. Engineering applications where compressive mean stresses occur as part of the applied stresses are rare. Therefore, other than for academic curiosity, there has not been a serious need for fatigue predictions under compressive mean loads.

With the recognition of the potential benefits of surface treatment processes, there is now a need for predicting fatigue behavior with compressive mean stresses. In the following section, application of a simple stress-strain function to unify available HCF data for different R-ratios and k values is developed. The resulting Fatigue Diagram is a modified Haigh Diagram that includes compressive mean stresses. This Fatigue Diagram enables (a) prediction of fatigue behavior in the presence of damage, (b) prediction of fatigue behavior in the presence of both damage and residual stresses, and (c) more importantly, provides a design guideline to determine the compressive residual stresses needed to achieve a target damage tolerance.

**MODEL DEVELOPMENT**

Smith et al<sup>18</sup> suggested a single stress-strain function,

$$(\sigma_{max}\epsilon_{alt}E) = \text{constant} \tag{4}$$

to combine the effects of mean stress and alternating stresses. This function, when plotted against  $\log(N_f)$ , was demonstrated to effectively unify the fatigue results for tensile and compressive mean stresses for SAE1015 steel, 2024-T4 Al alloy, SAE4340 steel and 24S-T3 Al alloy. Assuming that elasticity conditions dominate high cycle fatigue (and therefore  $\epsilon_{alt}E = \sigma_{alt}$ ). Fuchs and Stephens<sup>19</sup> considered application of the stress function,

$$(\sigma_{max}\sigma_{alt}) = \text{constant} \tag{5}$$

in place of the stress-strain function. Additionally, considering Neuber's rule<sup>20</sup> can include the effect of notches,

$$\sigma\epsilon = (k_f S)^2/E = k_f^2 S_e \tag{6}$$

where  $\sigma$  and  $\epsilon$  represent the notch root stress and strain, while S and e represent the nominal stress and strain, and  $k_f$  is the tensile notch severity factor (commonly known as the stress concentration factor, = notch root stress / nominal average stress). Equations 4, 5 and 6 lead to a new stress function

$$k_f(S_{max}S_{alt}) = \text{constant} \tag{7}$$

where  $k_f$  is the fatigue notch severity factor (= smooth bar fatigue strength / notched bar fatigue strength.)

Since  $S_{max} = S_{mean} + S_{alt}$ , the unifying stress function including the notch effects can be written as

$$k_f^2(S_{mean} + S_{alt})S_{alt} = \text{constant} \tag{8}$$

In the limiting case of  $k_f = 1$  and  $S_{mean} = 0$ , the constant is simply  $S_e^2$ , where  $S_e$  is the nominal fatigue strength (say, at a

fatigue life of  $10^7$  cycles) under fully-reversed cyclic loading ( $R = -1$ ) conditions. Therefore,

$$k_f^2(S_{mean} + S_{alt})S_{alt} = S_e^2 \quad [9]$$

Note: The terms  $k_t$  and  $k_f$  represent the tensile and fatigue notch severity factors, which are ratios of stresses without and with notch, and should not be confused with the stress intensity factor. Also, as Dowling<sup>20</sup> indicates,  $k_f < k_t$ .

Based on the above analysis, it is possible to theoretically construct a series of Haigh diagrams (modified Smith lines) for various  $k_f$  values, simply based on a single fatigue strength value,  $S_e$  for the material. Further, the series of lines when plotted within the bounds of O'Connor and Morrison's yield strength triangle, can provide engineering design limits. Fuchs and Stephens, when plotting this triangle, chose to use the cyclic yield stress for the maximum allowable alternating stress (apex of the triangle). For the purpose of this discussion, differences between the two choices are insignificant, since the locations of the relevant boundaries of interest are only marginally affected.

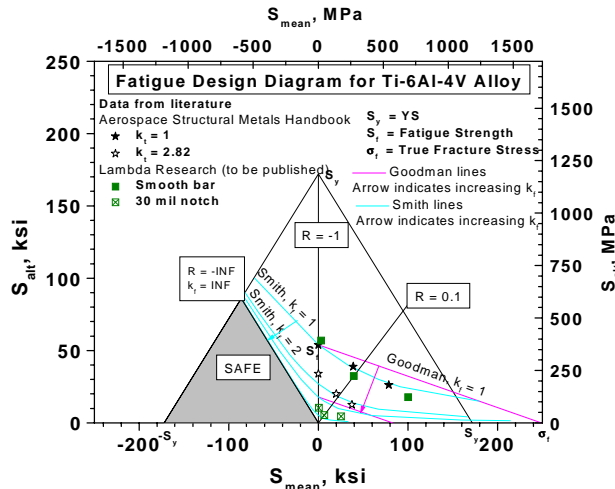


Figure 4 - Fatigue Design Diagram for Ti-6Al-4V alloy.

The Fatigue Diagram in Figure 4 illustrates this analysis for Ti-6Al-4V, as a plot of  $S_{alt}$  vs  $S_{mean}$ , with the yield strength triangle indicating the elastic limits. Fatigue strength data from Aerospace Structural Metals Handbook<sup>21</sup> for  $k_t$  values of 1 and 2.82 are plotted for R-ratios of -1, 0 and 0.5. Four-point bending fatigue results from tests conducted by the authors are also plotted. For the sake of reference, constant R-ratio lines for  $R = 0.1$ ,  $R = -1$  and  $R = -\infty$  are also plotted.

Goodman lines for  $k_f = 1$  and 3 were constructed using the fatigue strength value at  $R = -1$  and true fracture strength value from the Aerospace Structural Metals Handbook. Similarly, the modified Smith lines are plotted using the above equation and the single fatigue strength value,  $S_e$  at an R-ratio of -1 for the smooth bar, taken from the Aerospace Structural Metals

Handbook. The modified Smith line for  $k_f = 2$  shows a substantial debit in fatigue performance. The lines for  $k_f = 3$  and beyond practically converge in both the compressive and tensile mean stress regimes. For  $k_f \geq 5$ , and for the limiting notch condition ( $k_f$  approaching  $\infty$ ), the modified Smith line coincides with  $R = -\infty$  in the compressive mean stress region and shows practically no allowable alternating stress in the tensile mean stress regime. Within the triangular region marked "SAFE" in the Fatigue Diagram, to the left of  $R = -\infty$  ( $k_f = \infty$ ) line, the part is always in a fully compressed state. If the assumption that fatigue damage is not possible in the absence of tensile stresses is valid, then no fatigue damage is possible in this region.

For the sake of completeness, additional data from the HCF annual Report Section 2.2<sup>22</sup> are shown in Figure 5. As seen in this figure, there is general agreement between different sources of fatigue data in the mean stress regime corresponding to R-ratios of 0 and above, while in the mean stress regime with R-ratios  $< 0$ , there is some significant scatter in the data, and the modified Smith line under-predicts the reported fatigue strength.

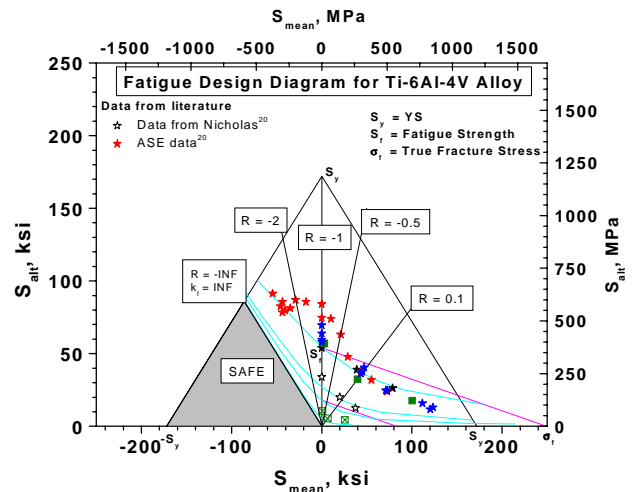


Figure 5. Same as Figure 4, with the inclusion of additional experimental data (smooth bar results) from reference 22.

**PREDICTION METHOD**

In using this Fatigue Diagram for design purposes, only the stresses in the region where fatigue damage initiation happens are of interest. For example, if the fatigue crack initiates from surface damage then local stresses in the affected region are of interest, including the immediate sub-surface region.

The knowledge of the fatigue loads (including R-ratio) and the target depth of required damage protection (say, 0.020 in.

deep FOD, or a 0.005 in. deep corrosion pit) are needed to design the depth and magnitude of the appropriate surface residual compressive layer. If no depth of damage protection is specified, the maximum achievable depth of damage protection analysis may be calculated for a given residual stress field.

In this section, a hypothetical case is discussed with the help of a magnified section of the Fatigue Design Diagram from Figure 6a. Let us assume that the component is subjected to fatigue loading at an R-ratio of 0.1. Modified Smith line for  $k_f = 1$  (no surface defects) predicts a nominal mean stress of 44 ksi and a nominal alternating stress of 36 ksi (Point A). In the presence of defects (at  $k_f = 3$ ), these values drop to about 15.4 and 12.6 ksi, respectively (Point B). In order to achieve full mitigation of the fatigue debit in the presence of the  $k_f = 3$  defect, the surface stress condition must be moved along the  $k_f = 3$  modified Smith line up to point C. The difference in the mean stress of Point C with respect to Point B (i.e., the distance BD) represents the amount of surface compressive residual stress needed at the bottom of the notch to fully mitigate the defective surface condition.

In a second example, let us consider a fatigue loading condition of  $R = -1$ . Under this condition, (Point A in Figure 6b) the modified Smith line for  $k_f = 1$  (smooth surface) predicts a  $S_{alt}$  of 54 ksi with a zero mean stress. For a limiting FOD condition of  $k_f = \infty$ , corresponding to even a modest size crack or notch, literally the fatigue strength falls to zero (Point B 6b). In order to achieve full mitigation for this condition, the surface (especially the FOD notch tip or crack tip) condition must be moved along the  $k_f = \infty$  modified Smith line to point C. Again, the difference in the mean stress of Point C with respect to Point B (i.e., the distance BD) represents the amount of surface compressive residual stress that must exist in the region covering the tip of the defect or crack to fully mitigate the fatigue debit.

**CASE STUDY OF MITIGATING FOD IN VANE-EDGE SIMULATION FEATURE SPECIMENS**

The following examples are taken from a study involving the HCF of vane-edge specimens, designed to simulate the fatigue conditions experienced by the trailing edge of a 1<sup>st</sup> stage compressor vane in a turbine engine. Figures 7(a) and (b) show two specimen designs for HCF testing at R-ratios of 0.1 and -1, respectively. All HCF tests were run in a Sonntag SF-1U fatigue machine with constant amplitude sinusoidal loading at 30 Hz and room temperature.

The Edges of these specimens were LPB treated to impart compressive residual stresses. Residual stresses were measured by X-ray diffraction methods and the results are plotted in Figure 8. This figure shows the full residual stress map as a function of distance (chord-wise) from the edge of the specimen. The mid-thickness is the least compressive site of

fatigue initiation, and is, therefore, of primary importance for design analysis. In Figure 8, the residual stress measurements were not limited only to the LPB treated region instead a full stress map is made to include the compensatory tension that ensues in regions behind the LPB processed regions. As seen in this figure, the maximum magnitude of compensatory tensile stresses (~ 32 ksi) are seen in the mid plane of the specimen just below the LPB processed region. Compensatory tensile stresses near the surface are lower. A more detailed discussion to incorporate the compensatory tension in the design is presented later in this paper.

Figure 9 shows the HCF test results in the form of S-N plots. In the presence of 0.020 in. FOD, the fatigue strengths at R-ratios of 0.1 and -1 are 10 and 15 ksi, respectively.

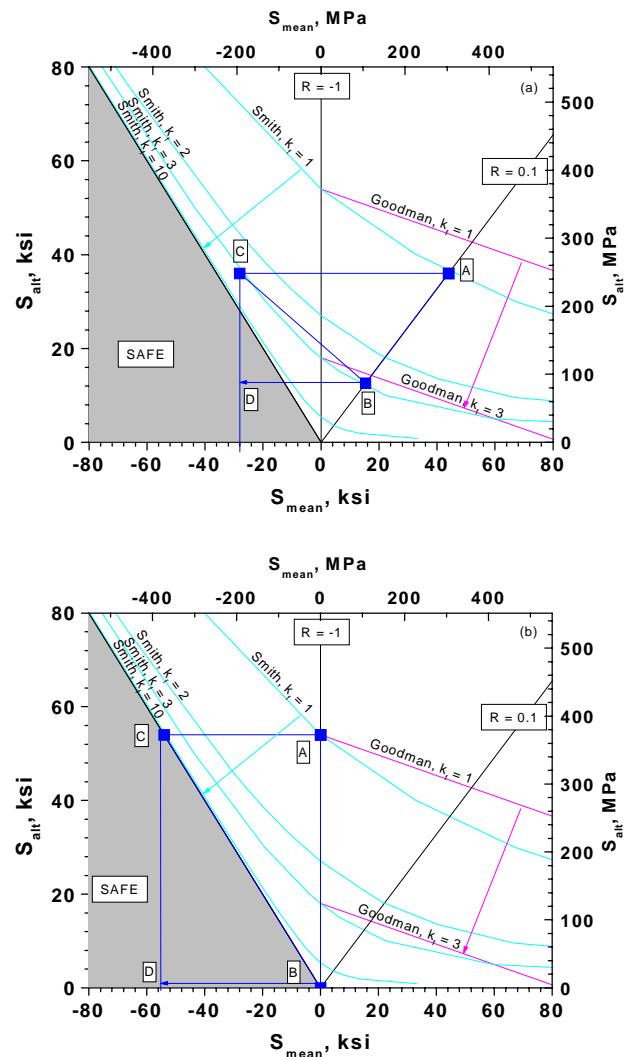


Figure 6 - Magnified sections of the Fatigue Design Diagram, with examples of the design process.

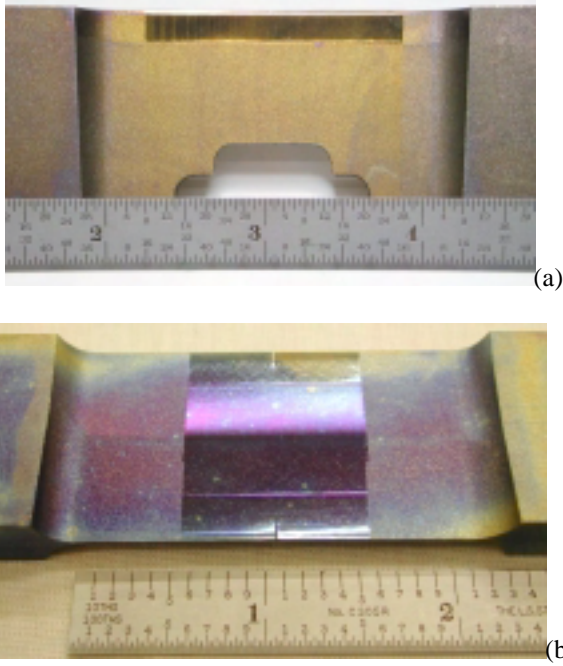


Figure 7(a) - Single Edge Blade (SEB) and (b) Double Edge Blade (DEB) feature specimens used for simulation of HCF damage in the trailing edge for HCF tests at R-ratio ( $\sigma_{min}/\sigma_{max}$ ) of 0.1 and -1.

None of the LPB treated specimens with FOD of 0.020 in. depth, tested at either R-ratio failed from FOD. Most specimens failed by sub-surface crack initiation from the mid-plane, as shown in Figure 10, indicating that the compression from LPB treatment mitigated the adverse effects of FOD. Further, in the absence of premature failure from compensatory tension in the sub-surface regions, an estimate of the surface initiated fatigue strength for LPB treated specimens with a 0.020 in. FOD at R = 0.1 was 110 ksi, and at R = -1, nominally 60 ksi.

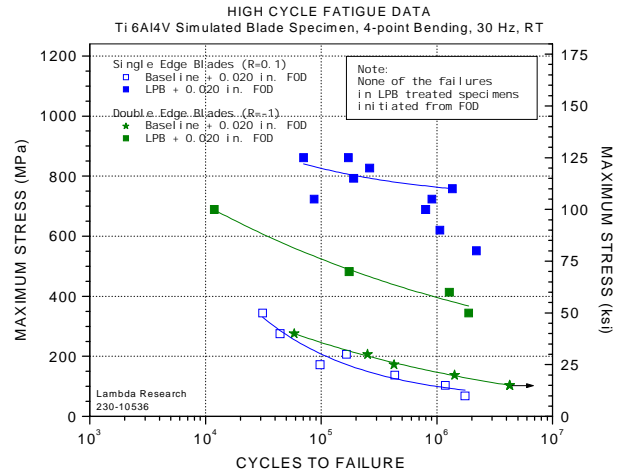


Figure 9. High cycle fatigue test results for the blade edge simulation feature specimens.

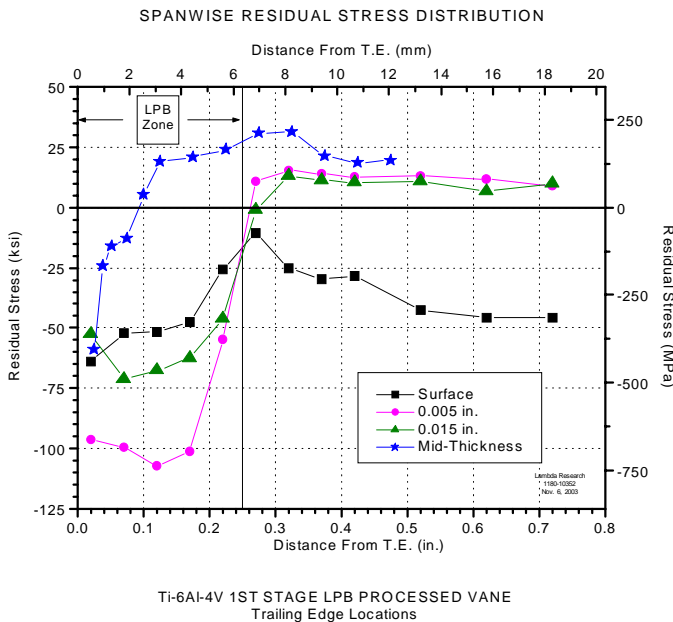


Figure 8 - Residual stress map of an LPB processed vane. This distribution represents X-ray diffraction measurements of spanwise residual stress at various distances from the trailing edge and depths from the surface.

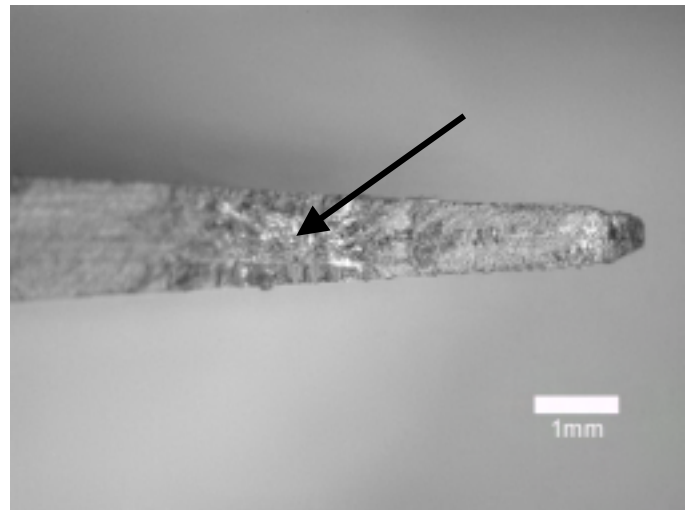


Figure 10 - Optical fractograph of a SEB feature specimen with LPB treatment showing crack initiation from sub surface regions (arrow). LPB + 0.02 in FOD, R = 0.1  $\sigma_{max}$  = 100 ksi,  $N_f$  = 800,038 cycles.

When plotted on the Fatigue Diagrams (Points B), shown in Figures 11a and 11b, the data points corresponded to a fatigue notch severity factor,  $k_f$  of 10 and 3.4 for R-ratios of 0.1

and  $-1$ , respectively. This difference in the  $k_f$  between the  $R$ -ratios for the same notch size may be attributed to the fatigue cycling conditions (tension-tension for  $R = 0.1$ , and tension-compression for  $R = -1$ ). Now, based on the knowledge of the mid-thickness compressive residual stresses from the LPB process at the tip of the 0.020 in. deep FOD, namely,  $-60$  ksi, points B can be translated to points C along the respective modified Smith lines. Position C in Figures 11a and 12a represent the actual combined (residual plus applied) stress state at the tip of the FOD. The applied stresses for the corresponding FOD tip stresses are represented by points E, which represents the predicted performance of these specimens. The estimated fatigue strengths of 110 ksi (for  $R = 0.1$ ) and 60 ksi (for  $R = -1$ ), in the absence of compensatory tension, are plotted in Figures 11a and 11b as points F (Actual). It is evident from Figures 11a and 11b that there is reasonable agreement between the predicted and actual data.

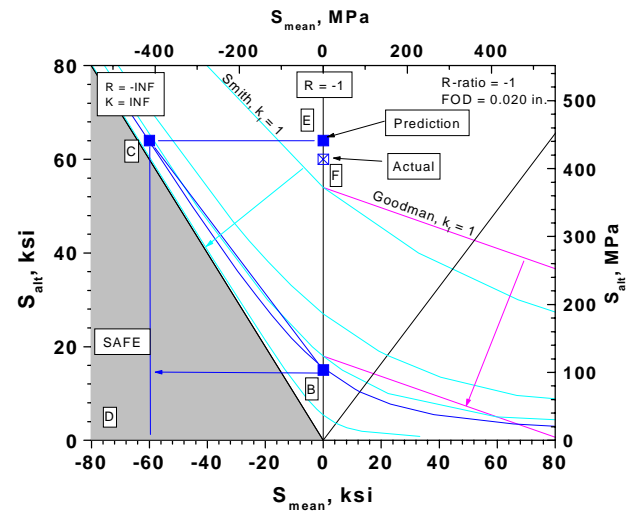


Figure 11b. Fatigue diagram depicting the benefits of LPB process at  $R = -1$ .

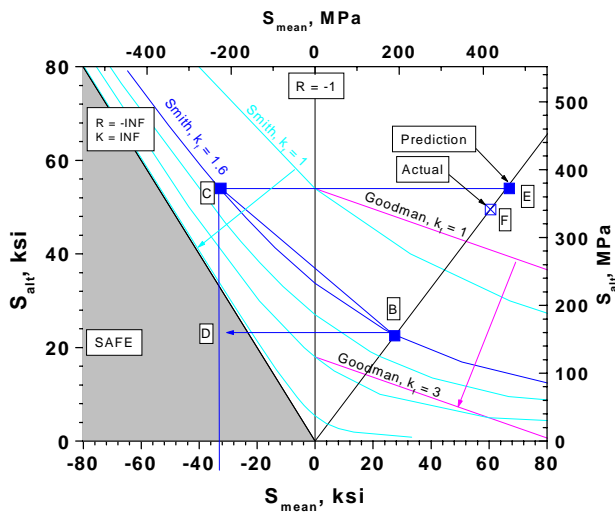


Figure 11a - Example of validation of the design process at  $R = 0.1$ .

However, none of the LPB treated specimens actually failed from the EDM simulated FOD. The failures came from sub-surface crack initiation where the compensatory tension stresses were maximum, the fatigue strength associated with this failure mode for  $R = 0.1$  and  $R = -1$  are determined to be 75 ksi and 45 ksi, respectively. When the presence of sub-surface compensatory tension of 32 ksi in the mid-thickness of the specimen is introduced (from Figure 8) into the Fatigue Diagram analysis, the corresponding results are presented in Figures 12a and 12b. The analytical procedure is identical to that presented in Figures 11a and 11b. Since the subsurface region has no obvious defects, the initial fatigue strength of the specimens are marked by point B in Figures 12a and 12b on the modified Smith line corresponding to  $k_f = 1$ . The compensatory

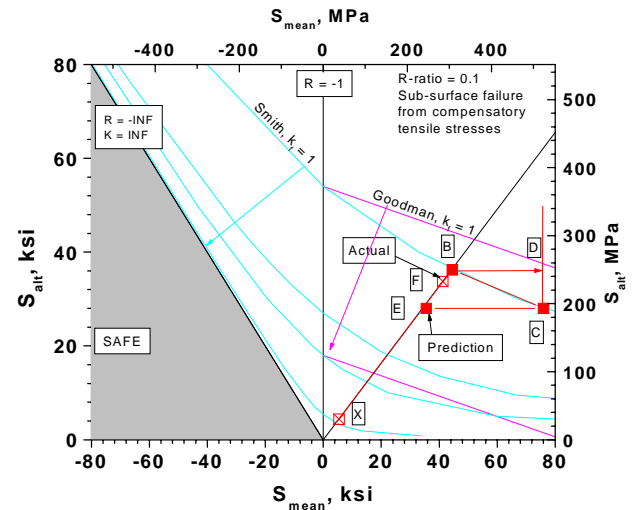


Figure 12a - Predictive analysis to account for the compensatory tension seen in Figure 8, for the fatigue test condition of  $R = 0.1$ .

tension in the sub-surface region (32 ksi) is accounted for by translating this point along the  $k_f = 1$  line to point C. Since the overall specimen is at an  $R$ -ratio of 0.1 and  $-1$ , respectively in Figures 12a and 12b, the points are translated to point E, which is the predicted fatigue strength under these conditions. Actual fatigue strengths measured experimentally, are marked by points F in Figures 12a and b.

It is evident from Figures 12a and 12b that the predicted fatigue strengths are lower than the predictions from 11a and 11b, confirmed by the observation of sub-surface crack initiation. In the absence of the LPB treatment, due to the presence of the 0.020 in. FOD, the fatigue strengths of the specimens were found to be corresponding to the points X in Figures 12a and 12b. Even with the sub-surface crack initiation

from the region with compensatory tension in the structure, the fatigue strengths of the specimens with LPB treatments were better by a factor of 3 and 5 times for  $R = -1$  and  $R = 0.1$ , respectively as compared to the specimens without treatment.

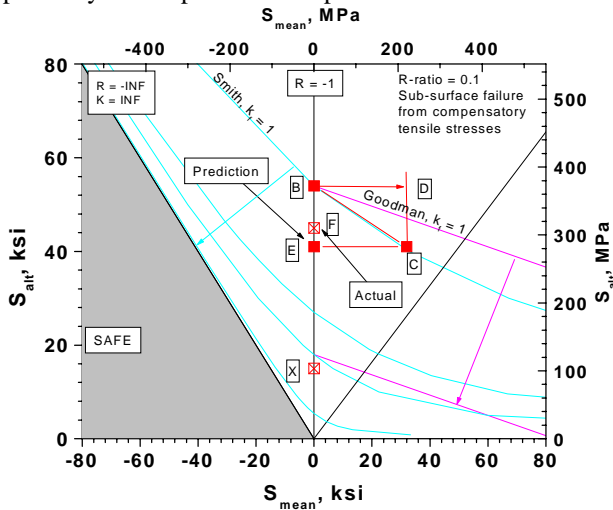


Figure 12b Predictive analysis to account for the compensatory tension seen in Figure 8, for the fatigue test condition of  $R = -1$ .

The small differences between predictions and actual results may be attributed to cumulative statistical scatter in both the residual stress measurements and fatigue test data. Further analyses in Ti-6Al-4V and other alloy systems are currently under way to further validate this predictive design procedure.

**WEIGHT SAVINGS AND OTHER DESIGN ISSUES**

The Fatigue Design Diagram analysis is presented in this paper mainly as a means of introducing compressive residual stress into the component design for the purpose of mitigating damage that may occur in service. However, this design method has the potential to provide significant material weight and cost savings, if used in the early stages of the design. As a simple example, let us consider a plate with a hole in the center loaded in tension with some superimposed vibratory stresses, say, at an R-ratio of 0.7. The allowable stress is the net section stress adjusted for the tensile notch severity factor,  $k_t$  (or fatigue notch severity factor,  $k_f$ ) of 3. For Ti-6Al-4V, the upper limit of the yield strength is nominally 172 ksi (1186 MPa), so a  $k_t$  of 3 reduces the maximum applied stress to 57 ksi (393 MPa).

The fatigue strength in the absence of the hole is represented by  $S_{max} = 143$  ksi (985 MPa), and in the presence of a hole ( $k_f = 3$ ) is reduced to,  $S_{max} = 47$  ksi (324 MPa). Correspondingly, the plate thickness would have to be tripled to meet design requirements. However, the introduction of a compressive residual stress of  $-50$  ksi ( $-345$  MPa) around the hole will restore the full fatigue strength. This is illustrated using the Fatigue Design Diagram in Figure 13. Points A, B, and C, represent the original fatigue strength, the loss of fatigue

strength due to introducing a hole, and the increase in the allowed alternating stress due to introducing the  $-50$  ksi compressive residual stress to restore the original fatigue strength, respectively. Taking full credit for the residual stress introduced in design saves nearly two-thirds of the material weight and cost.

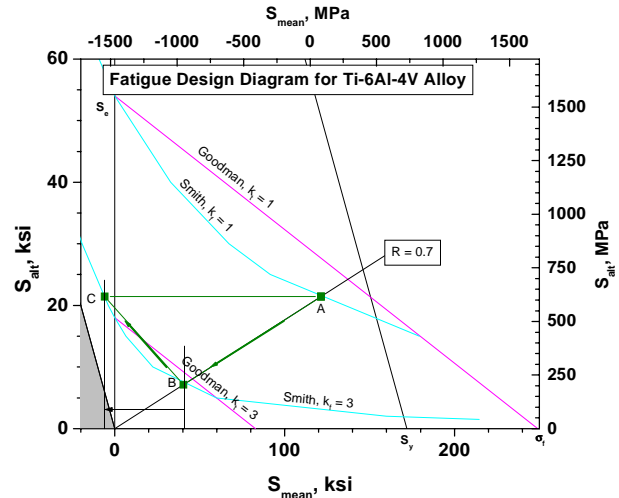


Figure 13. Section of the Fatigue Design Diagram illustrating the required magnitude of compression to fully mitigate the effect of FOD of  $k_f$  of 3.

**SUMMARY AND CONCLUSIONS**

In summary, a design method based on a modified Smith model for unifying high cycle fatigue data for various conditions of R-ratio and fatigue notch severity factor ( $k_f$ ) has been developed. A Fatigue Design Diagram (modified Haigh Diagram) – a map of mean stress vs. alternating stress to include both tensile and compressive mean stress regions, has been developed that allows accurate prediction of the effects of both compressive and tensile residual stresses on the high cycle fatigue performance of Ti-6Al-4V. A series of modified Smith lines for various  $k_f$  values to account for notch severity allows the prediction of fatigue safe zones. This in turn leads to the identification of the stress conditions for optimum and maximum fatigue benefits, including residual stresses.

Using the Fatigue Design Diagram, a design methodology to incorporate surface compressive residual stresses imparted through various surface treatments has been developed that allows the fatigue effects of the residual stresses present in the component to be included in the overall fatigue design. The method was validated through experimental results. This predictive methodology further reveals that deeper, higher compressive residual stresses may not always be useful in mitigating fatigue, because compensatory tension in other parts of the structure could play a crucial role in determining the ultimate benefits derived from the introduction of compressive

residual stresses. Therefore, the full effects of surface enhancement methods, including equilibrating tension, must be evaluated in order to take credit for residual compression in design.

## REFERENCES

1. Frost, N.E. Marsh, K.J. Pook, L.P., *Metal Fatigue*, Oxford University Press, 1974.
2. Fuchs, H.O. and Stephens, R.I., *Metal Fatigue In Engineering*, John Wiley & Sons, 1980.
3. Berns, H. and Weber, L., "Influence of Residual Stresses on Crack Growth," *Impact Surface Treatment*, edited by S.A. Meguid, Elsevier, 33-44, 1984.
4. Ferreira, J.A.M., Boorrego, L.F.P., and Costa, J.D.M., "Effects of Surface Treatments on the Fatigue of Notched Bend Specimens," *Fatigue, Fract. Engng. Mater., Struct.*, Vol. 19 No.1, pp 111-117, 1996.
5. Prev y, P.S. Telesman, J. Gabb, T. and Kantzos, P., "FOD Resistance and Fatigue Crack Arrest in Low Plasticity Burnished IN718", *Proceedings of the 5<sup>th</sup> National HCF Conference*, Chandler, AZ. March 7-9, 2000.
6. Clauer, A.H., "Laser Shock Peening for Fatigue Resistance," *Surface Performance of Titanium*, J.K. Gregory, et al, Editors, TMS Warrendale, PA (1996), pp 217-230.
7. P. Prev y, N. Jayaraman, R. Ravindranath, "Effect of Surface Treatments on HCF Performance and FOD Tolerance of a Ti-6Al-4V Vane," *Proceedings 8<sup>th</sup> National Turbine Engine HCF Conference*, Monterey, CA, April 14-16, 2003
8. Paul S. Prev y, Doug Hornbach, Terry Jacobs, and Ravi Ravindranath, "Improved Damage Tolerance in Titanium Alloy Fan Blades with Low Plasticity Burnishing," *Proceedings of the ASM IFHTSE Conference*, Columbus, OH, Oct. 7-10, 2002
9. Paul S. Prev y, et. al., "The Effect of Low Plasticity Burnishing (LPB) on the HCF Performance and FOD Resistance of Ti-6Al-4V," *Proceedings: 6<sup>th</sup> National Turbine Engine HCF Conference*, Jacksonville, FL, March 5-8, 2001.
10. M. Shepard, P. Prev y, N. Jayaraman, "Effect of Surface Treatments on Fretting Fatigue Performance of Ti-6Al-4V," *Proceedings 8<sup>th</sup> National Turbine Engine HCF Conference*, Monterey, CA, April 14-16, 2003
11. Paul S. Prev y and John T. Cammett, "Restoring Fatigue Performance of Corrosion Damaged AA7075-T6 and Fretting in 4340 Steel with Low Plasticity Burnishing," *Proceedings 6<sup>th</sup> Joint FAA/DoD/NASA Aging Aircraft Conference*, San Francisco, CA, Sept 16-19, 2002
12. N. Jayaraman, Paul S. Prev y, Murray Mahoney, "Fatigue Life Improvement of an Aluminum Alloy FSW with Low Plasticity Burnishing," *Proceedings 132<sup>nd</sup> TMS Annual Meeting*, San Diego, CA, Mar. 2-6, 2003.
13. Paul S. Prev y and John T. Cammett, "The Influence of Surface Enhancement by Low Plasticity Burnishing on the Corrosion Fatigue Performance of AA7075-T6," *Proceedings 5<sup>th</sup> International Aircraft Corrosion Workshop*, Solomons, Maryland, Aug. 20-23, 2002.
14. John T. Cammett and Paul S. Prev y, "Fatigue Strength Restoration in Corrosion Pitted 4340 Alloy Steel Via Low Plasticity Burnishing," Retrieved Sept. 2, 2003 from <http://www.lambda-research.com/publica.htm>.
15. Paul S. Prev y, "Low Cost Corrosion Damage Mitigation and Improved Fatigue Performance of Low Plasticity Burnished 7075-T6", *Proceedings of the 4th Int. Aircraft Corrosion Workshop*, Solomons, MD, Aug. 22-25, 2000.
16. S. Suresh, *Fatigue of Materials*, Cambridge University Press, 2001, p. 226-227
17. H.C. O'Connor, and J.L.M. Morrison, *International Conference on Fatigue*, Institution of Mechanical Engineers, 1956, pp 102-109.
18. K.N. Smith, P. Watson, and T.H. Topper, "A Stress-Strain function for the Fatigue of Metals", *Journal of Materials*, Vol. 5, No. 4, Dec. 1970, pp 767-778.
19. H.O. Fuchs and R.L. Stephens, "Metal Fatigue", John Wiley & Sons, New York, 1980, p.153.
20. N.E. Dowling, "Mechanical Behavior of Materials", Prentice Hall, New Jersey, 1999, p. 627
21. *Aerospace Structural Metals Handbook*, 3704
22. T. Nicholas (2001), 2.2 Air Force In-House Research (Fan & Turbine), *HCF Annual Report*

---

\* Design & Test Protocol Patent Pending